Chinese Journal of Polymer Science Vol. 33, No. 7, (2015), 964–975

Chinese Journal of Polymer Science
© Chinese Chemical Society
Institute of Chemistry, CAS
Springer-Verlag Berlin Heidelberg 2015

Effect of Microdomain Structure on the Mechanical Behavior of Binary Blends*

Bin Su, Yong-sheng Zhao, Feng Chen** and Qiang Fu**

College of Polymer Science and Engineering, State Key Laboratory of Polymer Materials Engineering, Sichuan University, Chengdu 610065, China

Abstract The relationship between microphase structure and mechanical response of the binary blends consisting of polystyrene-block-polyisoprene-block-polystyrene copolymer and low molecular weight polystyrene has been investigated. Low molecular weight polystyrene was chosen to obtain uniformly solubilized nano-blends without macrophase separation. The specimens were solution-cast by adding different amounts of homo-polystyrene to acquire different microphase structures. Small angle X-ray scattering (SAXS), transmission electron microscopy (TEM) and atom force microscopy (AFM) have been used to study the microdomain and grain structure. It is observed that the structural changes in *d*-spacing and grain size on account of different amounts of polystyrene alter the mechanical behavior in both monotonic tensile and cyclic tests. The elastic and the Mullins effects are strongly sensitive to the changes in *d*-spacing and grain sizes. Moreover, the sample with bi-continuous structure shows the largest tensile strength and Mullins effect. In addition, the Mooneye-Rivlin phenomenological model was used to evaluate and explore the relationship between the polymer topological networks and the rubber elasticity of these styrenic nano-blends.

Keywords: Microphase; Grain size; *d*-Spacing; Bi-continuous structure; Elastic response.

INTRODUCTION

Thermoplastic elastomers (TPEs) have been widely used because of their feature of both elasticity and thermoplasticity. One of the most important TPEs is a kind of block copolymers which are covalently jointed homopolymer chains. These materials undergo microphase separation upon cooling and form a series of nanoscale periodic structural hierarchy such as spheres, hexagonally packed cylinders, alternating lamellae *etc*. Cylindrical and lamellar systems form individual grains accompanied with grain boundaries. These microphase structures are influenced by the molecular composition f, the segment-segment interaction energy χ (the Flory-Huggins interaction parameter), and the degree of polymerization N, where χ is known to be inversely proportional to the temperature T. Many studies[1–4] on block copolymers have focused on describing their microphase structures and phase transitions. Hashimoto and co-workers[5–8] have been studying the microphase transitions of diblock copolymers and triblock copolymers since the last 1980s. They systematically studied the microphase structure change of styrene-isoprene block copolymers, such as: molecular-weight dependence and selective solvents dependence of lamellar and spherical microdomains. Futhermore, a highly ordered bicontinuous morphology named "tetrapod-network structure" was found for this diblock copolymers.

* This work was financially supported by the National Natural Science Foundation of China (Nos. 51173112 and 51121001) and the Special Funds for Major State Basic Research Projects of China (No. 2011CB606006).
** Corresponding authors: Feng Chen (陈枫), E-mail: fengchen@scu.edu.cn
Qiang Fu (傅强), E-mail: qiangfu@scu.edu.cn
Received October 27, 2014; Revised January 22, 2015; Accepted January 31, 2015
doi: 10.1007/s10118-015-1649-4

In addition to pure system, a more important and effective method to regulate the microphase structure is adding a homopolymer to a block copolymer whose chemical composition is similar with that for one of the blocks[9–13]. In such blends two different transitions can occur: macrophase and microphase separation. Which effect predominates depends on the relative lengths of the polymers and on the composition of the blend. When the ratio $r_A = M_A/M_{HA}$, where M_A and M_{HA} are the molecular weight of A block chains and the adding homopolymer A (HA), is sufficiently low, say 1, the low molecular weight homopolymer tends to be selectively and uniformly solubilized into the corresponding block copolymer microdomains, swelling the block chains or tends to localize in the middle of them. However, when r_A is high, for example far above 1, it tends to induce macrophase separation and thus the phase behavior of such blends can indeed become more complex. As has been reported, Richard and co-workers[14] investigated the ordered morphology of SI/PS by changing different conditions such as temperature, the molecular weight, and they can obtain an unusual structure which they called OBDD morphology. Han *et al*.[15] studied spatial distribution of the added homopolymer within the microdomain of mixtures of SBS/PS and SBS/PaMS. They found that the added homopolymer, PaMS or PS, was solubilized in the PS microdomains of SBS but the spatial distribution of the added homopolymer within the PS microdomains was different. The added PaMS was not distributed uniformly within the PS microdomains of SBS, whereas the added PS was distributed uniformly within the PS microdomains of SBS. Moreover, Hamley *et al*. and co-workers[16–20] did research on phase transitions of SIS/PS or SIS/PI binary blends. Their study has proven that blending is really an effective method to control the microphase structure of block copolymers.

As the morphology and mechanical properties of triblock copolymers are unique, studies on the relationship between them are quite significant from both fundamental and practical perspectives. However, relatively few studies[21–30] have focused on the mechanical response of triblock copolymers with various morphologies although there are lots of studies on characterizing morphological behavior. Huy and Michler[28, 29] have examined different deformation behavior of SBS block copolymers with different morphologies. They reported that the interfacial structure has a great impact on the deformation mechanism. Mamodia and Lesser[30] have investigated the effect of processing conditions on the structural characteristics and mechanical properties of a cylindrically microphase separated SEBS triblock copolymer, and they found that structural changes alter the mechanical behavior in both monotonic and cyclic tests. Zhao and Hotta *et al*.[31–32] did research on temperature dependent mechanical response of SIS triblock copolymer and reported that by varying processing temperature the block copolymer presents different microphase structure and the sample with long-range order has higher performance than that with short-range order or disordered structure. Molecular descriptions on the mechanism of rubber elasticity, the slip-tube model and Mooneye-Rivlin model for instance, have also been developed by several other groups[33, 34]. In addition, Lesser *et al*.[35] introduced a new approach to prepare a prestressed competitive double network in SBS, and the physical and mechanical properties of the network were studied. Kramer *et al*.[36] have shown that hexagonal cylinders with PS as the discrete domain can be achieved in a polystyrene-*b*-polyisoprene (PS−PI) miktoarm copolymers. These miktoarm materials are strong, tough, and elastic and may be potential candidates for a new generation of thermoplastic elastomers. There are studies[37–44] on the relationship between morphology and mechanical properties for binary blends consisting of a block copolymer and a homo-polymer where macrophase separation always occurs because of the large molecular weight of the homo-polymer. However, what effects the change in microphase structure such as *d*-spacing and grain sizes may have on the resulting mechanical behavior for the blends consisting of a block copolymer and a low molecular weight homopolymer still needs systematical study.

With this purpose, we did our research. We use a commercial SIS block copolymer blended with small amount of a low molecular weight polystyrene to investigate what structural parameters in these binary blends govern their elastic response. We focused on the relationship between the characteristic structural parameters and the elastic behaviors.

EXPERIMENTAL

Materials

In preparing binary blends of a block copolymer and a homopolymer, a commercial SIS triblock copolymer under the trade name Vector 4111 (Dexco Polymers Co.) was used, which has a weight-averaged molecular weight (M_w) of 1.4×10^5 g/mol, with a weight fraction of PS blocks of 0.183, and a polydispersity index (M_w/M_n) of 1.11. We also synthesized, *via* RAFT polymerization, a low molecular weight polystyrene (PS-4) having M_n = 4191 g/mol and M_w/M_n = 1.304. The number-average molecular weight of each polymer was determined by GPC. Table 1 gives a summary of sample codes and the molecular characteristics of the polymers employed in this study.

Table 1. Summary of the molecular characteristics of the polymers investigated in this study

Sample code	M_n [a] (g/mol)	M_w/M_n	WPS [c]	f [d]
(a) SIS triblock copolymer vector 4111	1.28×10^5	1.11	0.183	0.164
(b) Polystyrene PS-4	4.1×10^3	1.30	1	1

[a] Number-average molecular weight (M_n); [b] Polydispersity (M_w/M_n) determined by gel permeation chromatography; [c] Weight fraction of PS block (w_{PS}) determined by nuclear magnetic resonance spectroscopy; [d] Volume fraction of PS blocks (f) calculated at room temperature

Synthesis of Low Molecular Weight Polystyrene

Using living/controlled free radical polymerization, we synthesized homo-polystyrene (PS-4) using AIBN as initiator and toluene as solvent. The chain transfer agent we used was a kind of trithiocarbonate (RAFT), which was kindly supplied by the research group of Professor Ran, Sichuan University. The polymerization was terminated by addition of large amounts of degassed methanol into the reaction mixture. The solution was precipitated by addition of an excess amount of methanol. The precipitated polymer was filtered and dried at 70 °C for 3 days in a vacuum oven.

Sample Preparation (Solution Casting)

Samples were prepared by first dissolving a predetermined amount of Vector 4111 and PS-4 in toluene (10 wt% in solution) in the presence of 0.1 wt% antioxidant and then slowly evaporating the solvent. The evaporation of solvent was carried out initially at room temperature for 3–4 days and then in a vacuum oven at 40 °C for 12 h. The drying of the samples was continued until there was no further change in weight and then annealed in a vacuum oven for 12 h at 125 °C, which is well above $T_{g,PS}$ (101 °C). Table 2 gives a summary of sample codes and compositions of the Vector 4111/(PS-4) binary blends. In the following section, we will use SIS/PS-Φ briefly where Φ denotes the total volume fraction of PS in different blends. For example, SIS-0.16 denotes the pure Vector 4111, and SIS/PS-0.23 denotes the Vector 4111/(PS-4) whose total volume fraction of PS is 0.23.

Table 2. Sample code and composition for the Vector 4111/(PS-4) blends investigated

Sample code [a]	Total volume fraction of PS
100/0 Vector 4111 (PS-4)	0.16
91/9 Vector 4111 (PS-4)	0.23
82/18 Vector 4111 (PS-4)	0.30
73/27 Vector 4111 (PS-4)	0.37
64/36 Vector 4111 (PS-4)	0.44

[a] The numbers refer to the weight percent (*e.g.*, 91/9 Vector 4111/(PS-4) means 91 wt% Vector 4111 and 9 wt% PS-4)

Structure Analysis

Small angle X-ray scattering (SAXS) measurements were conducted to confirm the microphase-separated structures of each sample. The X-ray apparatus consisted of the X-ray generator with Cu Kα radiation of 0.154 nm, and a CCD detector was employed to collect two-dimensional (2D) SAXS patterns. The sample-to-detector distance was 2300 mm. A 2D area detector (RAPID) was used to record SAXS patterns. The morphology of the sample was determined by analyzing the relationship between the scattering intensity and the scattering vector q from 0 to 1 nm^{-1}.

Transmission electron microscopy (TEM) was conducted to investigate the morphology of the neat SIS and the binary blends. Ultrathin sections of ~80 nm thickness were obtained by cryomicrotoming at −100 °C to attain the rigidity of the specimen, using a Leica EMUC6/FC6 microtome. A transmission electron microscope (FEI-Tecnai G2 F20 S-TWIN) operated at 200 kV was used for taking pictures of the specimens after they were stained for 40 min in a ~2% aqueous solution of osmium tetroxide (OsO_4) that selectively stained the polyisoprene (PI) microdomains.

Atom force microscopy (AFM) (SPI4000, SIINT Instruments, Japan) was carried out to confirm the morphologies in tapping mode. Different mass ratios of Vector 4111 and PS-4 (Table 2) were first dissolved into toluene to get 3.23 wt% solutions, and the thin films were prepared by spin coating the solution onto mica at 2000 r/min for 30 s using a KW-4A commercial spin coater (XingYouYan, China). The spin-coated film was then annealed at 125 °C for 12 h in a vacuum oven before the AFM observation. Topographic and phase images were obtained simultaneously, however, only the phase images are presented as they have more contrast.

Monotonic Tensile and Cyclic Tests

Monotonic tensile tests and cyclic tests were performed on the same machine (Instron 5567) at 23 °C with a crosshead speed of 50 mm/min. The specimens with different morphologies were cut into a rectangle shape of 50 mm × 5 mm before the mechanical testing to create stress-strain curves and five specimens were tested for each group to provide a good statistical representation.

The elastic recovery test was evaluated by a step cycle test which combined a stepwise stretching of the samples with unloading-reloading cycles. The samples were strained to a prescribed strain and then cycled 3 times at that strain at a rate of 50 mm/min and later stepped to higher strain. The extension ratios λ^t = 1, 2, 3, 4 and 5.

RESULTS AND DISCUSSION

Structural Analysis by TEM

To confirm the exact microdomain morphologies of Vector 4111/(PS-4) mixtures, we independently carried out TEM for the samples. Figure 1 shows a series of TEM micrographs for SIS-0.16, SIS/PS-0.23, SIS/PS-0.30,

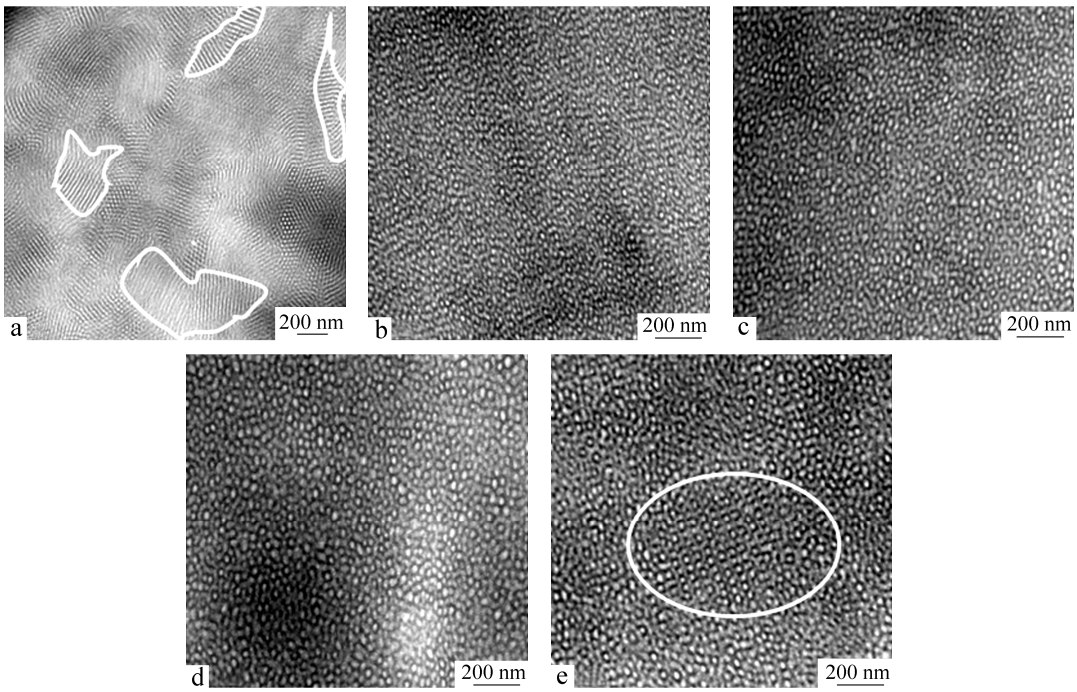

Fig. 1 TEM images of (a) SIS-0.16, (b) SIS/PS-0.23, (c) SIS/PS-0.30, (d) SIS/PS-0.37 and (e) SIS/PS-0.44 (200nm scale) (The dark regions represent the PI domains as OsO_4 selectively stains the isoprene phase.)

SIS/PS-0.37, and SIS/PS-0.44 mixture samples. In the TEM micrographs, the polyisoprene (PI) phase appears dark and the polystyrene (PS) phase appears bright since the staining agent OsO_4 used in the present work preferentially reacts with double bonds of the PI block. There are no aggregated bright areas in the TEM pictures which means that low molecular weight polystyrene has been completely solubilized into the corresponding block copolymer microdomains without macrophase separation. As clearly shown in Fig. 1(a), the pure SIS-0.16 displays the obvious hexagonally cylinders with long range order as has been shown in other studies[16, 19]. The white signed circle shown in Fig. 1(a) represents the grain size of the microstructure. However, the microstructure of blending samples lose the long range order with the addition of homo-polystyrene as shown in Figs. 1(b), 1(c), 1(d) and 1(e), which means that the grain size of these samples is much smaller than that of the pure SIS-0.16. In addition, compared with other samples, a special ordered structure could be seen in the sample SIS-0.44, as shown in Fig. 1(e). We can clearly see these special ordered structures in a large scale picture, as shown in Fig. 2. These structures might be referred to as a perforated lamellar (PL) or modulated lamellar (ML) phase structure, a kind of bi-continuous structure existing in the transient structure from hexagonally cylinders (HEX) to lamellae (LAM). Figure 3 illustrates the micro-mechanism of micro-separation of SIS and PS.

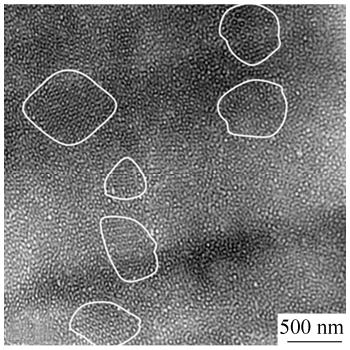

Fig. 2 A TEM image of SIS/PS-0.44

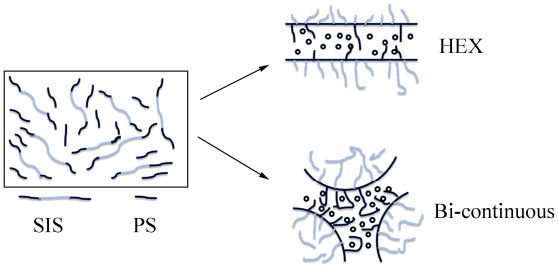

Fig. 3 A scheme to illustrate the micro-mechanism of SIS (Vector 4111) and PS

Structural Analysis by Small-angle X-ray Scattering

Small-angle-X-ray scattering (SAXS) was used to study the microphase-separated structures of the solution-cast films of Vector 4111/PS-4 binary blends. Figure 4(a) shows the SAXS profiles of different samples with different morphologies. Comparing with other samples with PS-4, the pure SIS-0.16 has stronger scattering peaks at $q = \sqrt{3}q_m$ and $q = \sqrt{4}q_m$ relative to that of the first-order scattering maxima q_m. This indicates a hexagonally packed cylindrical morphology of SIS-0.16, which is in accordance with the TEM picture. However, at higher concentrations of PS homopolymer (SIS/PS-0.23, SIS/PS-0.30, SIS/PS-0.37, SIS/PS-0.44) the sample display different SAXS patterns (Fig. 4a). The scattering peaks at $q = \sqrt{3}q_m$ and at $q = \sqrt{4}q_m$ recede obviously. This profile has been interpreted as an intermediate structure for diblock copolymer/homopolymer blends[42]. To be precise, this profile may indicate the intermediate structures from hexagonally packed cylindrical structures to lamella structure which can be seen at higher PS concentrations in binary blends. As Vaidya has reported, T_{ODT} (order-disorder temperature) of SIS/PS blends decreases with the increase of PS

homopolymer, so annealing at 125 °C will lead to micellae without long-range order if the T_{ODT} of SIS/PS blend is below or close to 125 °C[16]. That's why the microstructure of SIS/PS-0.23, SIS/PS-0.30, SIS/PS-0.37 and SIS/PS-0.44 shown in TEM pictures (Fig. 1) lose long-range order.

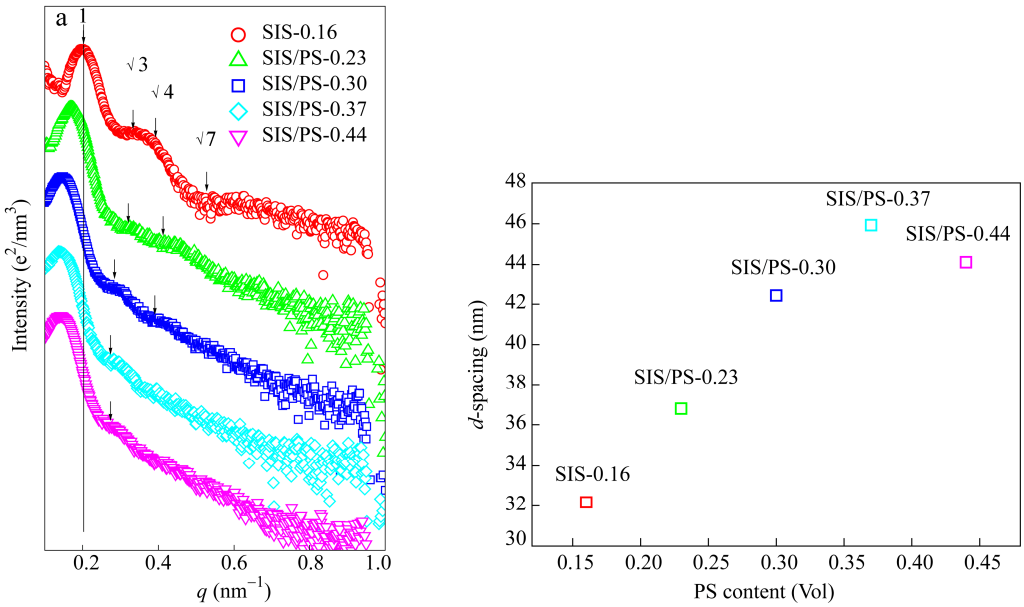

Fig. 4 (a) SAXS profiles for SIS-0.16, SIS/PS-0.23, SIS/PS-0.30, SIS/PS-0.37 and SIS/PS-0.44; (b) Change in *d*-spacing with different solution casting samples

It can be also seen from the Fig. 4(a) that different samples show different q_m, thus different *d*-spacing. The *d*-spacing is related to the distance between cylindrical domains as well as cylinder diameter, which is defined as *d*-spacing = $2\pi/q_m$. As shown in Fig. 4(b) we can see clearly the variation of *d*-spacing with different samples. The *d*-spacing increases consistently with the increase of PS content, which indicates that the added homo-polystyrene has been fully mixed with the PS blocks of SIS. However, the *d*-spacing of SIS/PS-0.44 is smaller than that of SIS/PS-0.37, presumably because of the formation of the bi-continuous structure in the sample SIS/PS-0.44.

Observation of Microphase-separated Structures by AFM

The microphase separation of Vector 4111/PS-4 spin-coated system was also confirmed by AFM as a complementary characterization. As shown in Fig. 5, the structure of different samples is clearly presented. Figure 5(a) shows a "fingerprint" structure formed by parallel domains. This is the typical structure of Vector 4111 which has been justified in many literatures[20, 31, 32]. However, with the adding of PS-4 to the Vector 4111, we can see a great change on surface structure of this thin film. As shown in Fig. 5(b), the interdomain distance of surface structure for SIS/PS-0.23 gets broad obviously although most of the PS cylinders still parallelly arrayed as the case in neat Vector 4111. As PS-4 were continuously added to Vector 4111, SIS/PS-0.30 and SIS/PS-0.37 display the coexistence of perpendicularly aligned and parallelly aligned cylinders, shown in Figs. 5(c) and 5(d). The orientation conversion from parallel orientation in SIS-0.16 and SIS/PS-0.23 to perpendicular cylinder orientation in SIS/PS-0.30 and SIS/PS-0.37 could be explained by the enthalpic increase, which is large enough to overcome the stability of the initial parallel cylinder orientation in SIS-0.16 and SIS/PS-0.23. It can be seen that adding low molecular weight PS to Vector 4111 can lead to more enthalpy which is favorable to the perpendicular orientation. However, as the total volume fraction of PS increases to 0.44, shown in Fig. 5(e), a complicated surface morphology rather than bi-continuous structure as shown in Fig. 1(e) appears. Figure 5(e) shows an irregular structure with a majority of connected PS domains. This might

be a transient state from the cylindrical to the lamellar morphology or "micellae without long-range order" according to Hamley who found the same phenomenon as ours[19]. It should be noted here that AFM images of thin film specimens spin coated at mica represent only the surface structure of the samples. There is a difference between surface and interior structure. Therefore, these AFM pictures for thin film samples can only be considered as a side characterization.

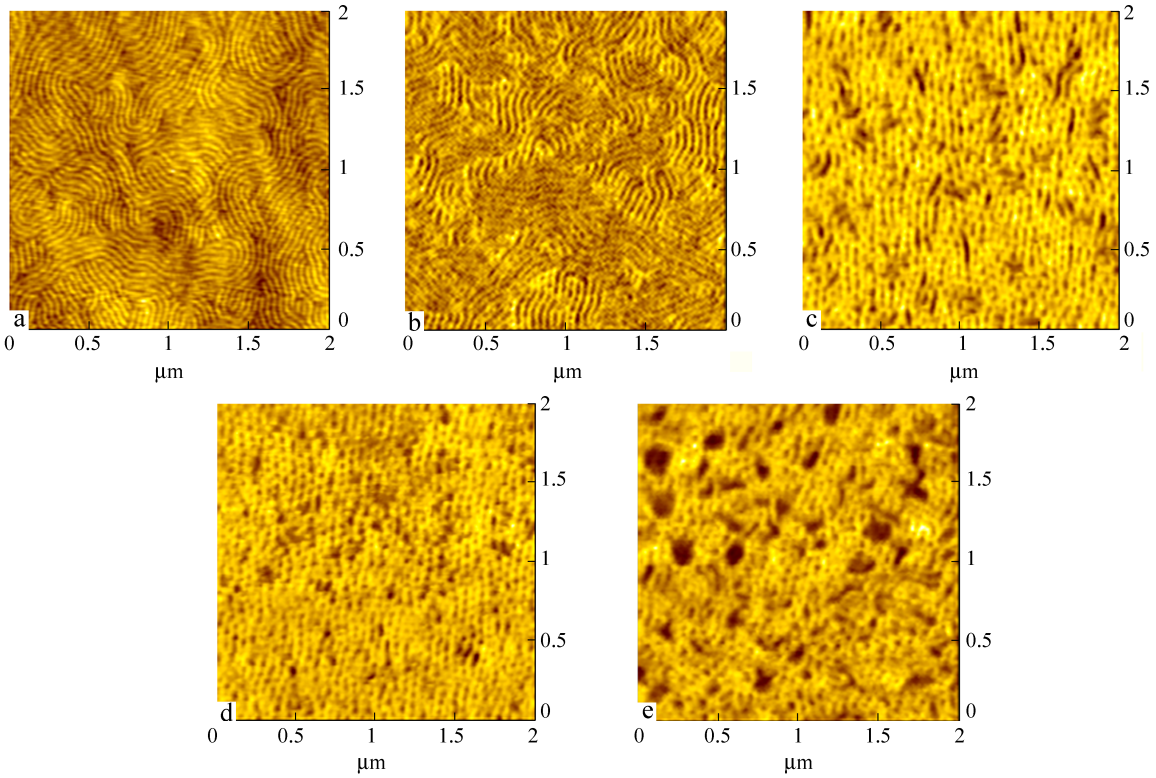

Fig. 5 AFM pictures of (a) SIS-0.16, (b) SIS/PS-0.23, (c) SIS/PS-0.30, (d) SIS/PS-0.37 and (e) SIS/PS-0.44

Monotonic Tension Response of Samples

The results of the nominal stress-strain measurements for samples are shown in Fig. 6. These solution cast specimens were stretched to a large strain (500%) instead of fracture because of the measuring range limitation of tensile testing machine. Table 3 lists the mechanical properties (Young's modulus and stress at 300% strain) for different specimens. The stress-strain curves of the samples as shown in Fig. 6 show an unusual trend which is not consistent with increasing PS content. As shown in Fig. 6, although the Young's modulus of the binary blends (SIS/PS-0.23, SIS/PS-0.30, SIS/PS-0.37, SIS/PS-0.44) increases with increasing PS content, the Young's modulus of the pure SIS-0.16 is higher than SIS/PS-0.23 and SIS/PS-0.30 and is close to SIS/PS-0.37. Moreover, the Young's modulus of SIS-0.44 is much larger than that of the other samples which may be due to a special structure in this sample. Figure 7 gives the trend of Young's modulus and stress at 300% strain of samples.

Table 3. Young's modulus and stress at 300% strain for different specimens

Samples	Young's modulus (MPa)	Stress at 300% strain (MPa)
SIS-0.16	1.84 ± 0.07	1.22 ± 0.06
SIS/PS-0.23	1.24 ± 0.02	1.04 ± 0.02
SIS/PS-0.30	1.38 ± 0.06	1.19 ± 0.03
SIS/PS-0.37	1.80 ± 0.11	1.85 ± 0.07
SIS/PS-0.44	2.59 ± 0.07	2.42 ± 0.07

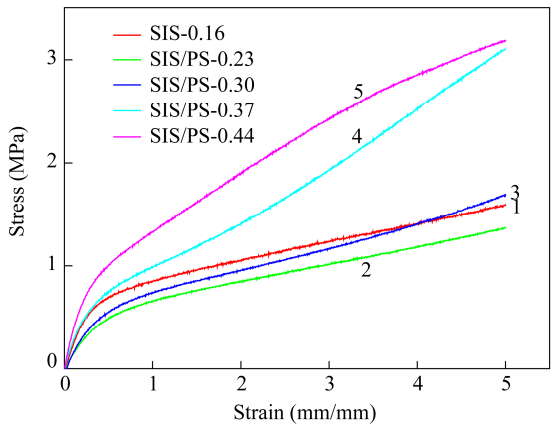

Fig. 6 Tensile stress-strain relations of the solution casting specimens with different PS contents at ambient temperature

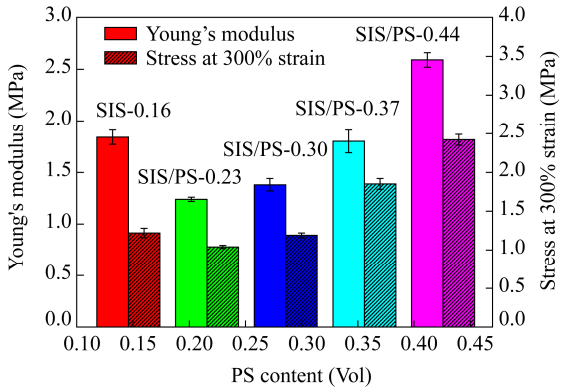

Fig. 7 Change in Young's modulus and stress at 300% strain of different solution casting samples

As has been reported[31, 32], the tensile deformation process began with the orientation and fracture of the hard component and followed by rubber elasticity of the soft segment. Therefore, the morphology-mechanical property relationship of triblock copolymers can be investigated by the structural balance between the hard segment and the soft segment. As shown in Fig. 1(a), the grain size is larger than that of other samples, which denotes that the structure consistency of SIS-0.16 is larger than that of other samples. That's the reason why the Young's modulus of the pure SIS-0.16 is higher than that of SIS-0.23, SIS-0.30 and is close to that of SIS-0.37 though the *d*-spacing of SIS-0.16 is the lowest. For the samples SIS/PS-0.23, SIS/PS-0.30 and SIS/PS-0.37 whose grain sizes are almost the same, Young's modulus increases consecutively with the increase of the *d*-spacing, which corresponds with the study by Lesser *et al*[30]. They found that the Young's modulus of solution cast samples increases in proportion to the *d*-spacing value. Our experiment results testify this viewpoint deeply. However, when the volume fraction of PS increases to 0.44, the grain size and the *d*-spacing are not the predominant factor for Young's modulus any more because of the formation of the bi-continuous structure in this sample. As has been reported, samples with double gyroid (one kind of bi-continuous structure) show higher mechanical properties than samples with other structures because double gyroid is a 3-dimensionally interpenetrating periodic structure[45]. A higher extent of continuous PS paths in the direction of loading exists in this bi-continuous structure. Therefore, the enhancement in mechanical properties of SIS/PS-0.44 is essentially due to the special 3D microdomain morphology of the bi-continuous structure.

Cyclic Behavior

Cyclic tests were performed on the samples to examine the elastic recovery. Figure 8 shows the stress-strain curves of the loading and unloading cycles of different samples. Mullins effect, the pronounced stress softening

during cyclic deformation, can be clearly seen in Fig. 8. As shown in Fig. 8, the ongoing loading or unloading never traced the previous loading or unloading curves. The sample SIS-0.16 has a bigger tensile modulus and shows larger Mullins effect than SIS/PS-0.23 and SIS/PS-0.30, which is in accordance with the tensile strength shown in Fig. 6. Moreover, the Mullins effect of samples SIS/PS-0.37 and SIS/PS-0.44 is more distinct than that of SIS-0.16, SIS/PS-0.23 and SIS/PS-0.30 and these samples show obvious strain hardening after several cycles which is attributed to the high PS content that leads to a transition from elastomer to plastomer. This phenomenon indicates that the sample SIS/PS-0.37 and SIS/PS-0.44 have a softer elastic response under cyclic deformation.

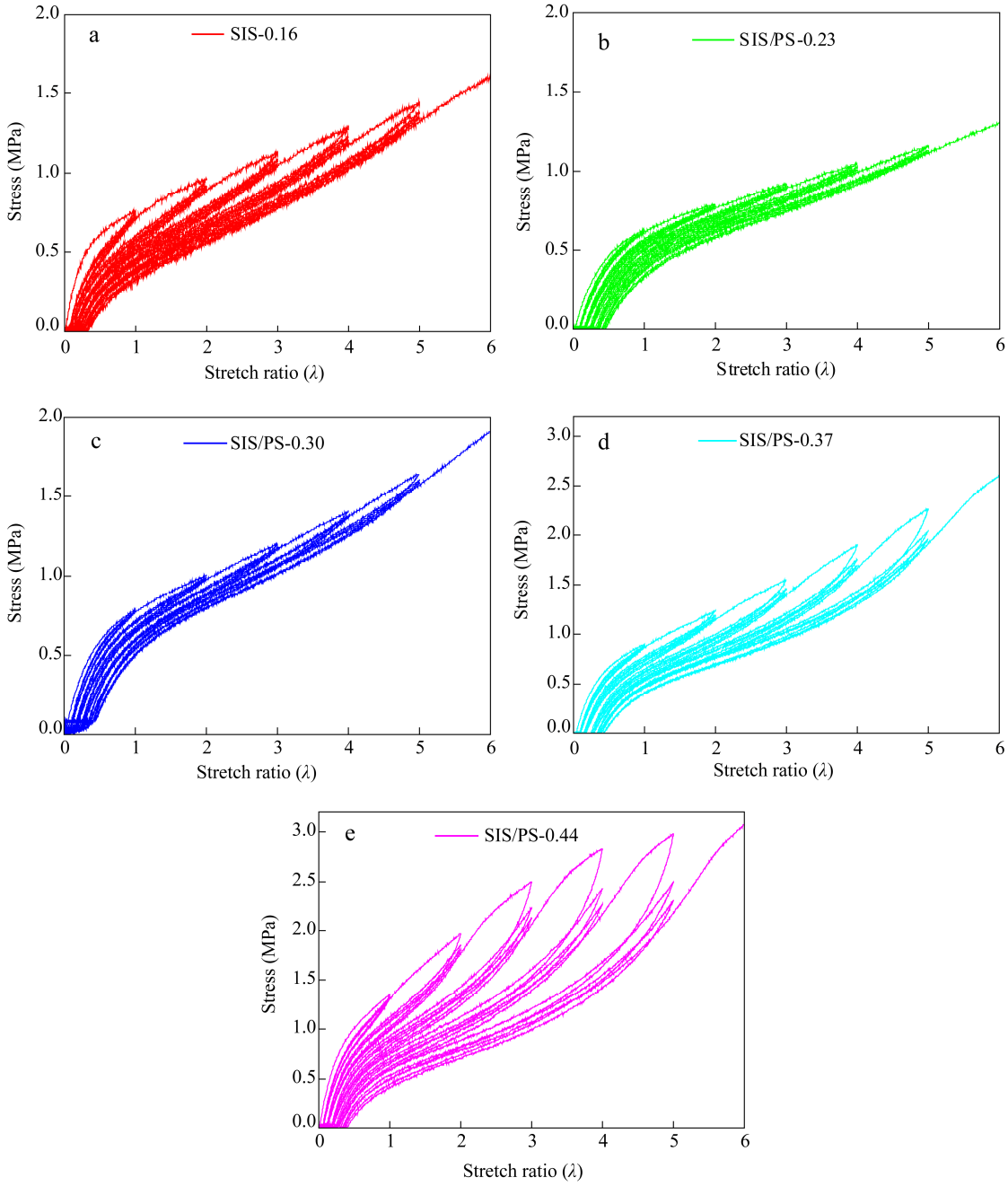

Fig. 8 Cyclic tests of different solution casting samples

As a previous study indicated[30], the extent of Mullins effect is associated with the relative stiffness of individual cylindrical domains, which depends on its diameter and modulus. Therefore, the extent of Mullins effect strongly depends on the domain diameter which is directly related to the *d*-spacing and grain size. Hence, the sample SIS-0.16 shows a larger Mullins effect than SIS/PS-0.23 and SIS/PS-0.30 is because of the high PS continuity caused by the large grain size of the microstructure. In addition, when the PS content increases to 0.37, the *d*-spacing rather than the grain size has become a predominant factor controlling the Mullins effect. That's the reason why the sample SIS/PS-0.37 and SIS/PS-0.44 display stronger Mullins effect than other samples do. It should be noted that the extent of Mullins effect and strain hardening of sample SIS/PS-0.44 is the strongest among all the samples. This phenomenon may be related to the unique 3D microdomain morphology of the bi-continuous structure in this sample which has the highest PS continuity compared with all other samples.

Rubber Elasticity of Topological Networks

There are some classical models predicting the stress-strain relationship of polymer networks. The statistical theory of rubber elasticity proposed by Flory predicts the nonlinear behavior at large strains of a rubber in uniaxial extension is given by

$$\sigma = G(\lambda - \lambda^{-2}) \tag{1}$$

where σ is the nominal stress, λ is the extension ratio, and G is the shear modulus. It should be in mind that the Flory theory does not take into account of trapped entanglement. In addition, Mooney and Rivlin[46, 47] proposed a semiempirical equation, which quantifies the deviation of the stress-strain relation relative to the prediction from Gaussian rubber elasticity

$$\sigma = 2(C_1 + C_2/\lambda)(\lambda - \lambda^{-2}) \tag{2}$$

where C_1 and C_2 are two material coefficients. Moreover, the Mooney stress, defined by

$$\sigma_R = \sigma/(\lambda - \lambda^{-2}) \tag{3}$$

depend on the deformation while it does not for the simple affine model.

Due to the same trend of different samples, Figure 9(a) only shows the experimental curves (the solid line) and predicted curves (the dashed line) based on Eq. (1) of SIS/PS-0.44 for simplicity. While the experimental and predicted curves are identical until $\lambda = 1.3$ (same Young's modulus), they have a big difference at higher strains: the slope of the experimental curve decreases sharply (softening). It should be noted that the stress-strain relationship deviates downward from the predicted curve based on Eq. (1) because of the presence of trapped entanglements. Thus we can conclude that the statistical theory of rubberlike elasticity can not predict the nonlinear behavior of the samples used in our experiments at large strains in uniaxial extension.

Figure 9(b) shows the Mooneye-Rivlin plots of different samples. Curves of SIS-0.16, SIS/PS-0.23 and SIS/PS-0.30 nearly show a neo-Hookean material behavior in the range at $0.2 < 1/\lambda < 0.7$, while the curves of SIS/PS-0.37, SIS/PS-0.44 show a linear range at $0.5 < 1/\lambda < 0.7$, which is corresponding to the low deformation region. This means that SIS-0.16, SIS/PS-0.23 and SIS/PS-0.30 behave as ideal elastomer in the entire deformation range compared to other samples. There are small differences for SIS/PS-0.37 and SIS/PS-0.44. With decreasing the inverse of stretch ratio, Mooney stress of SIS/PS-0.37 drops sharply and then decreases slowly nearly on a plateau at large deformation and then increases again, illustrating the softening followed by the hardening. However, SIS/PS-0.44 drops sharply and then decreases slowly without an increasing. It should be noted that entanglements play a dominant role in the elasticity of the materials at small strains, while PS cross-links become important for samples under large deformation. SIS/PS-0.37 and SIS/PS-0.44 derivate obviously from the prediction of Eq. (2) because of the presence of trapped entanglements which is due to the high PS content. Therefore, we can conclude that the Mooney and Rivlin semiempirical equation can be a good fit for low PS content networks (SIS-0.16, SIS/PS-0.23 and SIS/PS-0.30) but an inferior fit for high PS content networks (SIS/PS-0.37, SIS/PS-0.44).

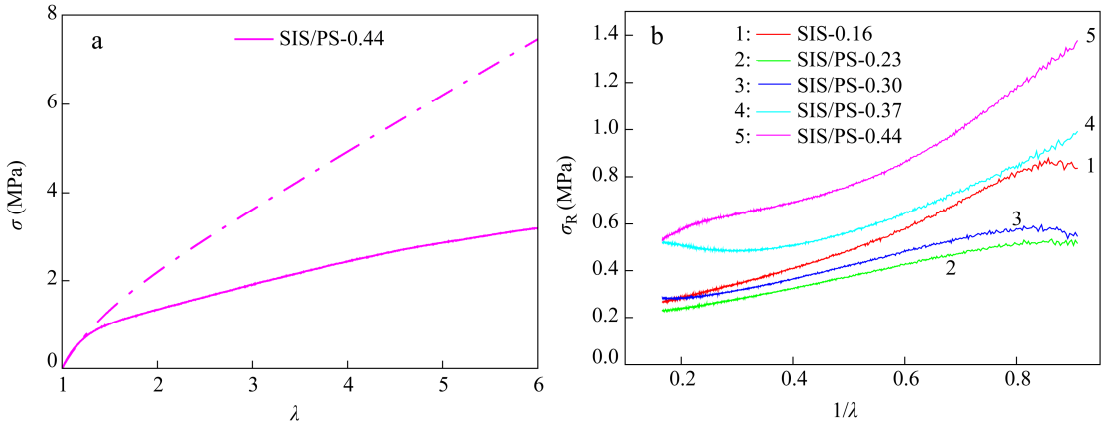

Fig. 9 (a) Stress-strain relationship of SIS/PS-0.44 (The dashed line is the fitting result of Eq. (1)); (b) Mooney-Rivlin plot of different samples

CONCLUSIONS

The influence of the low molecular weight polystyrene on the microstructure and the mechanical properties of poly (styrene-isoprene-styrene) triblock copolymer were investigated. Our results demonstrate a clear relationship between a measurable structural parameter and the mechanical response of styrenic thermoplastic elastomers and their binary blends with PS. The adding of low molecular weight polystyrene could regulate both the grain size and the *d*-spacing of microstructure. In addition, a rare bi-continuous microstructure has been discovered in our sample SIS/PS-0.44 and it denotes a strong mechanical response than other samples because of the unique 3-dimensionally network. Samples with low volume fraction of PS (SIS/PS-0.23, SIS/PS-0.30) display lower tensile strength and Young's modulus and Mullins effect than pure SIS-0.16 due to the large grain size of SIS-0.16. Furthermore, the modulus and Mullins effect of samples with moderate volume fraction of PS (SIS/PS-0.23, SIS/PS-0.30, SIS/PS-0.37) increase with increasing the *d*-spacing. The sample with high volume fraction of PS (SIS/PS-0.44) shows higher tensile strength and Young's modulus and high Mullins effect than other samples due to the 3-dimensionality of the PS network connectivity. Moreover, the Mooneye-Rivlin approach rather than the statistical theory can be a good fit equation to study the rubber elasticity of the samples investigated in our study.

ACKNOWLEDGEMENTS We would like to thank Prof. Liangbin Li for his help in SAXS experiments.

REFERENCES

1 Leibler, L., Macromolecules, 1980, 13: 1617
2 Ohta, T. and Kawasaki, K., Macromolecules, 1986, 19: 2632
3 Thomas, E.L., Lescanec, R.L., Frank, F.C., Higgins, J.S., Klug, A. and Hamley, I., Philos. Trans.: Phys. Sci. Eng., 1994, 348: 166
4 Xia, Y., Chen, J., Shi, T. and An, L., Chinese J. Polym. Sci., 2013, 31(9): 1249
5 Hashimoto, T., Macromolecules, 1980, 13: 1247
6 Hashimoto, T., Macromolecules, 1980, 13: 1669
7 Hashimoto, T., Macromolecules, 1987, 20: 1662
8 Shibayama, M., Hashimoto, T. and Kawai, H., Macromolecules, 1983, 16: 28
9 Tanaka, H. and Hashimoto, T., Macromolecules, 1991, 24: 5720
10 Han, C.D., Beak, D.M. and Kim, J., Macromolecules, 1992, 25: 3067

11 Beak, D.M. and Han, C.D., Macromolecules, 1992, 25: 3714
12 Spontak, R.J., Smith, S.D. and Ashraf, A., Macromolecules, 1993, 26: 5124
13 Choi, S, Lee, K.M. and Han, C.D., Macromolecules, 2003, 36: 803
14 Spontak, R.J., Smith, S.D. and Ashraf, A., Macromolecules, 1993, 26: 962
15 Kimishima, K. and Hashimoto, T., Macromolecules, 1995, 28: 3853
16 Vaidya, N.Y., Han, C.D. and Kim, D., Macromolecules, 2001, 34: 234
17 Choi, S., Lee, K.M. and Han, C.D., Macromolecules, 2003, 36: 803
18 Choi, S., Lee, K.M. and Han, C.D., Macromolecules, 2000, 33: 7083
19 Mykhaylyk, T.A., Mykhaylyk, O.O., Collins, S. and Hamley, I.W., Macromolecules, 2004, 37: 3377
20 Ahn, D.U. and Sancaktar, E., Adv. Funct. Mater., 2006, 16: 1958
21 Adhikari, R., Michler, G.H. and Knoll, K., Polymer, 2004, 45: 246
22 Miquelard, G.G., Hourdet, D. and Creton, C., Polymer, 2009, 50: 490
23 Mamodia, M., Indukuri, K., Atkins, E.T., Jeu, W.H.D. and Lesser, A.J., J. Mater. Sci., 2008, 43: 7046
24 Chong, H.M. and Taylor, A.C., J. Mater. Sci., 2013, 48: 6777
25 He, Y., Xie, D. and Zhang, X., J. Mater. Sci., 2014, DOI 10.1007/s10853-014-8458-y
26 Fu, Z., Gui, Y., Cao, C., Liu, B., Zhou, C. and Zhang, H., J. Mater. Sci., 2014, 49: 2874
27 Liang, D., Zhou, L., Zhang, Q., Chen, F., Wang, K., Deng, H. and Fu, Q., Chinese J. Polym. Sci., 2012, 30(4): 612
28 Huy, T.A., Adhikari, R. and Michler, G.H., Polymer, 2003, 44: 1257
29 Huy, T.A., Hai, L.H., Adhikari, R., Weidisch, R., Michler, G.H. and Knoll, K., Polymer, 2003, 44: 1245
30 Mamodia, M., Panday, A., Gido, S. P. and Lesser, A.J., Macromolecules, 2007, 40: 7328
31 Orimo, Y. and Hotta, A., Macromolecules, 2011, 44: 5317
32 Zhao, Y.S., Ning, N., Hu, X., Li, Y., Chen, F. and Fu, Q., Polymer, 2012, 53: 4317
33 Rubinstein, M. and Panyukov, S., Macromolecules, 2002, 35: 6686
34 Akagi, Y., Katashima, T., Katsumoto, Y., Fujii, K., Matsunaga, T. and Chung, U.I., Macromolecules, 2011, 44: 5821
35 Singh, N.K. and Lesser, A.J., Macromolecules, 2011, 44: 1490
36 Shi, W., Lynd, N.A., Montarnal, D., Luo, Y., Fredrickson, G.H. and Kramer, E.J., Macromolecules, 2014, 47: 2043
37 Adhikari, R., Huy, T.A., Henning, S., Michler, G.H. and Knoll, K., Collid. Polym. Sci., 2004, 282: 1391
38 Adhikari, R., Michler, G.H. and Knoll, K., Macromol. Symp., 2003, 198: 134
39 Adhikari, R., Michler, G.H., Godehardt, R. and Ivan'kova, E.M., Polymer, 2003, 44: 8051
40 Adhikari, R., Michler, G.H. and Knoll, K.M., Polymer, 2004, 45: 246
41 Adhikari, R., Buschnakowski, M., Lebek, W., Godehardt, R., Michler, G.H., Calleja, F.J.B. and Knoll, K., Polym. Adv. Technol., 2005, 16: 182
42 Adhikari, R., Huy, T.A., Buschnakowski, M., Michler, G.H. and Knoll, K., New J. Phys., 2004, 6: 28
43 Adhikari, R. and Michler, G.H., Prog. Polym. Sci., 2004, 29: 986
44 Bodycomb, J., Yamaguchi, D. and Hashimoto, T., Macromolecules, 2000, 33: 5197
45 Dair, B.J., Honeker, C.C., Alward, D.B., Avgeropoulos, A., Hadjichristidis, N., Fetters, L.J., Caple, M. and Thomas, E.L., Macromolecules, 1999, 32: 8152
46 Roos, A. and Creton, C., Macromolecules, 2005, 38: 7818
47 Akagi, Y., Katashima, T., Katsumoto, Y., Fujii, K., Matsunaga, T., Chung, U., Shibayama, M. and Sakai, T., Macromolecules, 2011, 44: 5821